Final version published as: Yuzwa, S. A., Cheung, A. H., Okon, M., McIntosh, L. P., & Vocadlo, D. J. (2014). O-GlcNAc Modification of tau Directly Inhibits Its Aggregation without Perturbing the Conformational Properties of tau Monomers. Journal of Molecular Biology, 426(8), 1736–1752. https://doi.org/10.1016/j.jmb.2014.01.004

O-GlcNAc Modification of tau Directly Inhibits Its Aggregation without Perturbing the Conformational Properties of tau Monomers

Scott A. Yuzwa[1,2,†], Adrienne H. Cheung[3,†], Mark Okon[3], Lawrence P. McIntosh[3] and David J. Vocadlo[1,2]

*1 - **Department of Molecular Biology and Biochemistry,** Simon Fraser University, 8888 University Drive, Burnaby, BC, Canada V5A 1S6*
*2 - **Department of Chemistry,** Simon Fraser University, 8888 University Drive, Burnaby, BC, Canada V5A 1S6*
*3 - **Department of Biochemistry and Molecular Biology,** Department of Chemistry, and the Michael Smith Laboratories, University of British Columbia, 2350 Health Sciences Mall, Vancouver, BC, Canada V6T 1Z3*

***Correspondence to David J. Vocadlo:** Department of Molecular Biology and Biochemistry, Simon Fraser University, 8888 University Drive, Burnaby, BC, Canada V5A 1S6. dvocadlo@sfu.ca*
http://dx.doi.org/10.1016/j.jmb.2014.01.004

Abstract

The aggregation of the microtubule-associated protein tau into paired helical filaments to form neurofibrillary tangles constitutes one of the pathological hallmarks of Alzheimer's disease. Tau is post-translationally modified by the addition of *N*-acetyl-D-glucosamine O-linked to several serine and threonine residues (*O*-GlcNAc). Previously, increased O-GlcNAcylation of tau has been shown to block the accumulation of tau aggregates within a tauopathy mouse model. Here we show that *O*-GlcNAc modification of full-length human tau impairs the rate and extent of its heparin-induced aggregation without perturbing its activity toward microtubule polymerization. O-GlcNAcylation, however, does not impact the "global-fold" of tau as measured by a Förster resonance energy transfer assay. Similarly, nuclear magnetic resonance studies demonstrated that O-GlcNAcylation only minimally perturbs the local structural and dynamic features of a tau fragment (residues 353–408) spanning the last microtubule binding repeat to the major GlcNAc-acceptor Ser400. These data indicate that the inhibitory effects of *O*-GlcNAc on tau aggregation may result from enhanced monomer solubility or the destabilization of fibrils or soluble aggregates, rather than by altering the conformational properties of the monomeric protein. This work further underscores the potential of targeting the *O*-GlcNAc pathway for potential Alzheimer's disease therapeutics.

Introduction

The aggregation of the microtubule-associated protein tau to form paired helical filaments, which ultimately give rise to neurofibrillary tangles (NFTs), is one of the two pathological hallmarks of Alzheimer's disease (AD). Given that the extent of NFTs correlates closely with progression of AD, there has been increasing attention on the molecular processes that influence the formation of tau aggregates. Understanding the processes that contribute to the ability of tau to form ordered aggregates is a critical step toward finding ways to block their formation. A basic nucleation-dependent mechanism, first proposed by Oosawa and Kasai to describe the kinetic behavior of actin polymerization [1], has been shown to accurately model the aggregation of tau [2,3] and other proteins contributing to neurodegeneration such as amyloid-β [4], α-synuclein [5], and the prion protein [6]. In the nucleation-dependent polymerization mechanism, the rate-limiting step is the formation of a minimal nucleus composed of a small number of monomers. This nucleus is then extended during an elongation phase until eventually the polymer reaches an equilibrium with respect to the concentration of monomeric species in solution. In the case of tau, a conformational change is thought to be a prerequisite for its aggregation [7,8]. Studies aimed at characterizing the structural properties of tau and the effects of tau post-translational modifications could therefore provide critical insights into the processes regulating fibril formation.

One post-translational modification that has been proposed as a driving force for tau fibril formation is

serine and threonine phosphorylation, which is generally accepted as preceding its fibrillization *in vivo* [9]. Tau, however, is also subject to a number of other post-translational modifications including, for example, proteolysis [10–12], acetylation [13], glycation [14,15], and O-glycosylation by O-linked *N*-acetyl-D-glucosamine (*O*-GlcNAc) [16]. The formation of *O*-GlcNAc involves the attachment of GlcNAc to the hydroxyl group of serine and threonine residues, and this modification is found on a diverse array of nucleocytoplasmic proteins. The addition of *O*-GlcNAc to proteins is catalyzed by a single glycosyltransferase, *O*-GlcNAc transferase (OGT) [17,18]. Similarly, its removal is catalyzed by a single glycoside hydrolase, *O*-GlcNAcase (OGA) [19,20]. The dynamic nature of O-GlcNAcylation, in that it can be added to and removed from a particular protein multiple times during its lifespan, makes this modification similar in some regard to protein phosphorylation [21]. However, whereas the role of phosphorylation on the aggregation of tau has been studied in detail [22–25], that of *O*-GlcNAc is poorly defined.

Various studies have suggested that *O*-GlcNAc present on tau plays a role in AD. First, Lefebvre *et al.* and Liu *et al.* have demonstrated that human tau is indeed *O*-GlcNAc modified and that O-GlcNAcylation can be reciprocal to tau phosphorylation [26,27]. Increased *O*-GlcNAc on tau is correlated with decreased phosphorylation and *vice versa*, at least in cell culture and *ex vivo* in tissue slices [26,27]. Second, Robertson *et al.* have shown that the *O*-GlcNAc levels of a tau-enriched fraction from the AD brain are significantly reduced as compared to age-matched healthy controls [28] and NFTs appear to completely lack *O*-GlcNAc [27]. This is notable because UDP-GlcNAc, the sugar donor substrate used by OGT, is derived from cellular glucose [29], which makes *O*-GlcNAc levels sensitive to changes in metabolism [30]. Given that impairment of glucose utilization in the AD brain is well described [31], it has been proposed [27] that decreased glucose utilization in the AD brain gives rise to lower UDP-GlcNAc levels, which in turn result in lower levels of tau O-GlcNAcylation and consequently higher levels of tau phosphorylation [27]. We initially speculated that, if one could *increase* levels of *O*-GlcNAc *in vivo*, tau phosphorylation might be reduced, which in turn could slow tau-driven neurodegeneration.

To test this hypothesis *in vivo*, we used Thiamet-G, a potent and selective OGA inhibitor, to increase *O*-GlcNAc levels on tau in the brains of JNPL3 transgenic mice [32]. This mouse model expresses a mutant form of human tau that becomes hyperphosphorylated and aggregates within the brain and spinal cord to form NFTs [33]. We found that treatment of these transgenic mice with Thiamet-G led to a decrease in the number of NFTs in their brains and spinal cords but did not prevent tau hyperphosphorylation [32]. We cannot, however, rule out changes in tau phosphorylation at specific sites not studied in that work. We further showed that *O*-GlcNAc modification of a truncated form of recombinant tau, devoid of phosphorylation, inhibited its aggregation *in vitro* [32]. Collectively, these data suggest that *O*-GlcNAc on tau may act to directly inhibit its aggregation. However, more detailed studies on the role of *O*-GlcNAc on aggregation of different human tau constructs, including the full-length protein, have not been performed.

To address whether *O*-GlcNAc modification of tau can influence its aggregation, we have recombinantly produced the longest human isoform of tau (Tau441) in both its unmodified and its *O*-GlcNAc-modified states. Using this material, we show that *O*-GlcNAc modification inhibits tau aggregation *in vitro*. Further, we find that this decreased rate of tau aggregation does not appear to be due to global structural changes in monomeric tau prior to its aggregation. In support of this conclusion, nuclear magnetic resonance (NMR) spectroscopic studies using a fragment of tau (residues 353–408) confirm minimal local structural and dynamic changes in the disordered polypeptide upon *O*-GlcNAc modification. Collectively, these data suggest that the effects of *O*-GlcNAc on tau aggregation result from enhanced monomer solubility or the destabilization of fibrils or soluble aggregates, rather than by altering the conformational properties of the monomeric protein.

Results and Discussion

Sample preparation

As shown previously, we have demonstrated that *O*-GlcNAc-modified Tau441 can be made recombinantly by co-expression of OGT and Tau441 in *Escherichia coli* [34]. However, while useful for mapping *O*-GlcNAc modification sites, this material was insufficiently pure to allow informative biochemical studies. To obtain higher purity *O*-GlcNAc-modified tau, we have now used high-performance liquid chromatography (HPLC) to produce both control Tau441 ($cTau441_{wt}$, expressed with the catalytically inactive H558A OGT mutant, mutOGT) and *O*-GlcNAc-modified Tau441 ($ogTau441_{wt}$, expressed with wild-type OGT, wtOGT) having a high level of purity and an absence of degradation products (Fig. 1a). We have also investigated a mutant form of Tau441 that has the major site of O-GlcNAcylation (Ser400) [34–36] mutated to alanine. This mutant tau was expressed recombinantly with mutOGT and wtOGT to produce control S400A Tau441 ($cTau441_{S400A}$) and *O*-GlcNAc-modified S400A Tau441 ($ogTau441_{S400A}$), respectively (Fig. 1a). Immunoblotting with a pan-specific *O*-GlcNAc antibody (CTD110.6) indicated that the S400A mutation resulted in approximately 2-fold less

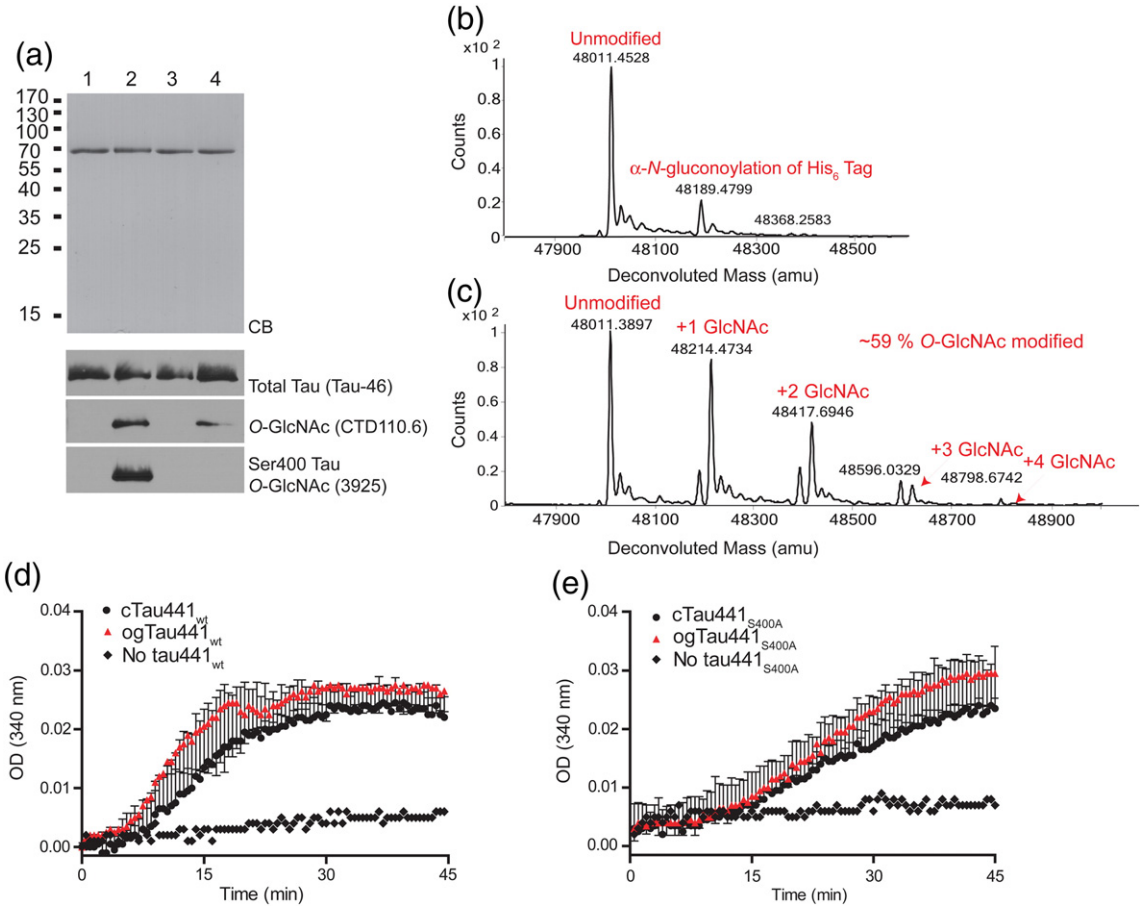

Fig. 1. Production of *O*-GlcNAc Tau441 and catalysis of microtubule polymerization. (**a**) Coomassie blue (CB)-stained SDS-PAGE gel (upper panel): Lane 1, cTau441$_{wt}$; Lane 2, ogTau441$_{wt}$; Lane 3, cTau441$_{S400A}$; and Lane 4, ogTau441$_{S400A}$. Total tau (Tau-46) immunoblot also indicates equal tau loading in all lanes. *O*-GlcNAc immunoblot with the pan-specific *O*-GlcNAc antibody, CTD110.6, indicates that only ogTau441$_{wt}$ and ogTau441$_{S400A}$ bear *O*-GlcNAc and that *O*-GlcNAc levels are ~50% lower in the ogTau441$_{S400A}$ sample. Finally, the Ser400 *O*-GlcNAc tau antibody, 3925, only detects *O*-GlcNAc at Ser400 on the ogTau441$_{wt}$ sample. ESI-MS reconstructed mass spectra of (**b**) cTau441$_{wt}$ and (**c**) ogTau441$_{wt}$ indicate that the ogTau441$_{wt}$ contains ~60% *O*-GlcNAc. The (*) symbol identifies the α-N-gluconoylated peaks. (**d**) Tubulin polymerization assays of cTau441$_{wt}$ and ogTau441$_{wt}$ indicate that *O*-GlcNAc does not impair or enhance microtubule polymerization. (**e**) Tubulin polymerization assays of cTau441$_{S400A}$ and ogTau441$_{S400A}$ also show that reduced *O*-GlcNAc levels do not affect microtubule polymerization.

O-GlcNAc on ogTau441$_{S400A}$ *versus* ogTau441$_{wt}$. This is consistent with Ser400 being a major site of modification by OGT. Electrospray ionization mass spectrometry (ESI-MS) of cTau441$_{wt}$ (Fig. 1b) and ogTau441$_{wt}$ (Fig. 1c) showed that the latter contains ~60% *O*-GlcNAc and ~40% unmodified Tau441$_{wt}$. On average, the population of *O*-GlcNAc-modified Tau441 had ~1.5 *O*-GlcNAc residues per protein molecule. We also detected a signal of 178 Da increased mass that is consistent with some (<20%) α-N-gluconoylation of the His$_6$-tag [37] of both the cTau441$_{wt}$ and the ogTau441$_{wt}$. The extent of this modification, which is known to occur on proteins recombinantly produced in *E. coli* [37–40], did not differ between the cTau441$_{wt}$ and the ogTau441$_{wt}$ (Fig. 1b and c).

Tubulin polymerization is independent of tau O-GlcNAcylation

To date, the only clearly assigned functions of tau are to bind to and stabilize microtubules [41]. For this reason, we were interested in whether *O*-GlcNAc modification of tau might alter its ability to affect microtubule polymerization. We therefore assayed the capacity of cTau441$_{wt}$ and ogTau441$_{wt}$ to promote tubulin polymerization and observed that both enhanced tubulin polymerization to similar extents (Fig. 1d). cTau441$_{S400A}$ and ogTau441$_{S400A}$ also showed no significant difference in their ability to enhance the rate of, or extent of, tubulin polymerization (Fig. 1e). However, the S400A mutation resulted in an approximately 3-fold decrease in the growth rate

of the tubulin polymer, as compared to wild-type Tau441, even though both $Tau441_{S400A}$ and $Tau441_{wt}$ were used at equivalent concentrations. These values were obtained by fitting the tubulin polymerization curves to a Gompertz model of growth [42].

O-GlcNAcylation inhibits Tau441 aggregation

We previously showed that *O*-GlcNAc on a truncated form of tau inhibits its aggregation *in vitro* [32]. To test whether *O*-GlcNAc acts to inhibit aggregation of full-length Tau441, we conducted *in vitro* aggregation assays using solutions containing both 10 μM tau and 10 μM heparin. Because of the unusually highly charged nature of tau and its paucity of aromatic amino acid residues, which makes tau behave differently from other proteins in many assays, careful measurement of its concentration prior to conducting the aggregation assays is important. As described below in Materials and Methods, this was achieved using three different approaches. Aggregation of these carefully standardized samples was then monitored by fluorescence spectroscopy using Thioflavin-S (ThS), which is known to bind preferentially to tau aggregates over tau free in solution [43]. Both $cTau441_{wt}$ and $ogTau441_{wt}$ aggregated over a period of 3 days with no readily apparent lag phase, and the resulting data were well fit to a single exponential growth curve. However, $ogTau441_{wt}$ aggregated more slowly and reached an equilibrium (plateau) value ~1.3-fold lower than that of $cTau441_{wt}$ (Fig. 2a). To probe this result via an independent method, we used an established filter-trap assay [44]. We found that this assay also detected a similar ~1.3-fold lower equilibrium position for $ogTau441_{wt}$ as compared to $cTau441_{wt}$ (Fig. 2b). Given that tau aggregates via a nucleation-dependent mechanism, the equilibrium position in such a model is controlled by the post-nuclear extension and contraction of tau fibrils. These data thus suggest that *O*-GlcNAc reduces the extension rate or increases the contraction rate of tau fibrils.

The observation that there is only ~60% *O*-GlcNAc-modified Tau441 in the $ogTau441_{wt}$ samples may obscure aspects of the observed aggregation. To acquire more detailed information, we set out to enrich further the quantity of *O*-GlcNAc-modified Tau441 in the $ogTau441_{wt}$ sample. Prior to enrichment, we also cleaved the His_6-tag from tau using thrombin to eliminate any potential impact of the tag and the small quantity of α-N-gluconoylated product mentioned above. To remove unmodified tau from this $ogTau441_{wt}$ sample, we conducted another round of HPLC purification using a very shallow gradient of 30–35% acetonitrile:water. These chromatography conditions resulted in two distinct peaks (Fig. 3a) that we speculated arose from *O*-GlcNAc-modified and unmodified Tau441 within the $ogTau441_{wt}$ preparations. Analysis of these fractions by immunoblotting using the Tau-46 antibody, which recognizes the C-terminus of tau, and the tau *O*-GlcNAc-Ser400 antibody 3925 [34] revealed that the earlier eluting peak was indeed due to *O*-GlcNAc-modified Tau441, whereas the later eluting peak stemmed from unmodified Tau441 present within the sample (Fig. 3a). The ability of such a small number of monosaccharides to influence the hydrophobicity of full-length tau, as reflected in these differences in chromatographic mobility, is striking. When the fractions corresponding to the earlier eluting peak were combined and compared to the $ogTau441_{wt}$ samples used in studies shown in Fig. 1, we found an approximately 2-fold enrichment in *O*-GlcNAc as estimated by immunoblotting (Fig. 3a and b). We

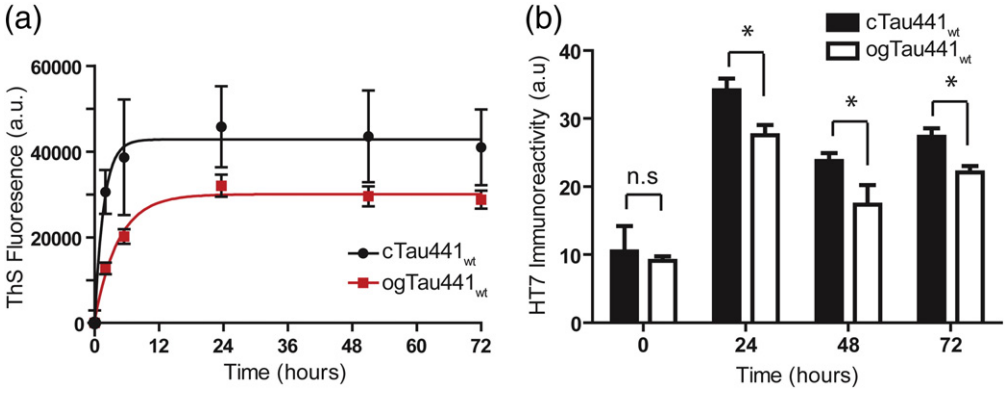

Fig. 2. *O*-GlcNAc modification causes slower aggregation of Tau441. (**a**) ThS binding assay of $cTau441_{wt}$ and $ogTau441_{wt}$ aggregation over a period of 3 days using 10 μM protein and 10 μM heparin. The $ogTau441_{wt}$ aggregates more slowly than $cTau441_{wt}$ and reaches a lower equilibrium plateau value. (**b**) Filter-trap assay of $cTau441_{wt}$ and $ogTau441_{wt}$ aggregation also demonstrates that $ogTau441_{wt}$ reaches an equilibrium position that is ~1.3-fold lower than $cTau441_{wt}$. $^*P < 0.05$ (two-tailed unpaired *t*-test), whereas n.s indicates not significant. Error bars represent standard error of the mean and lines represent exponential fits.

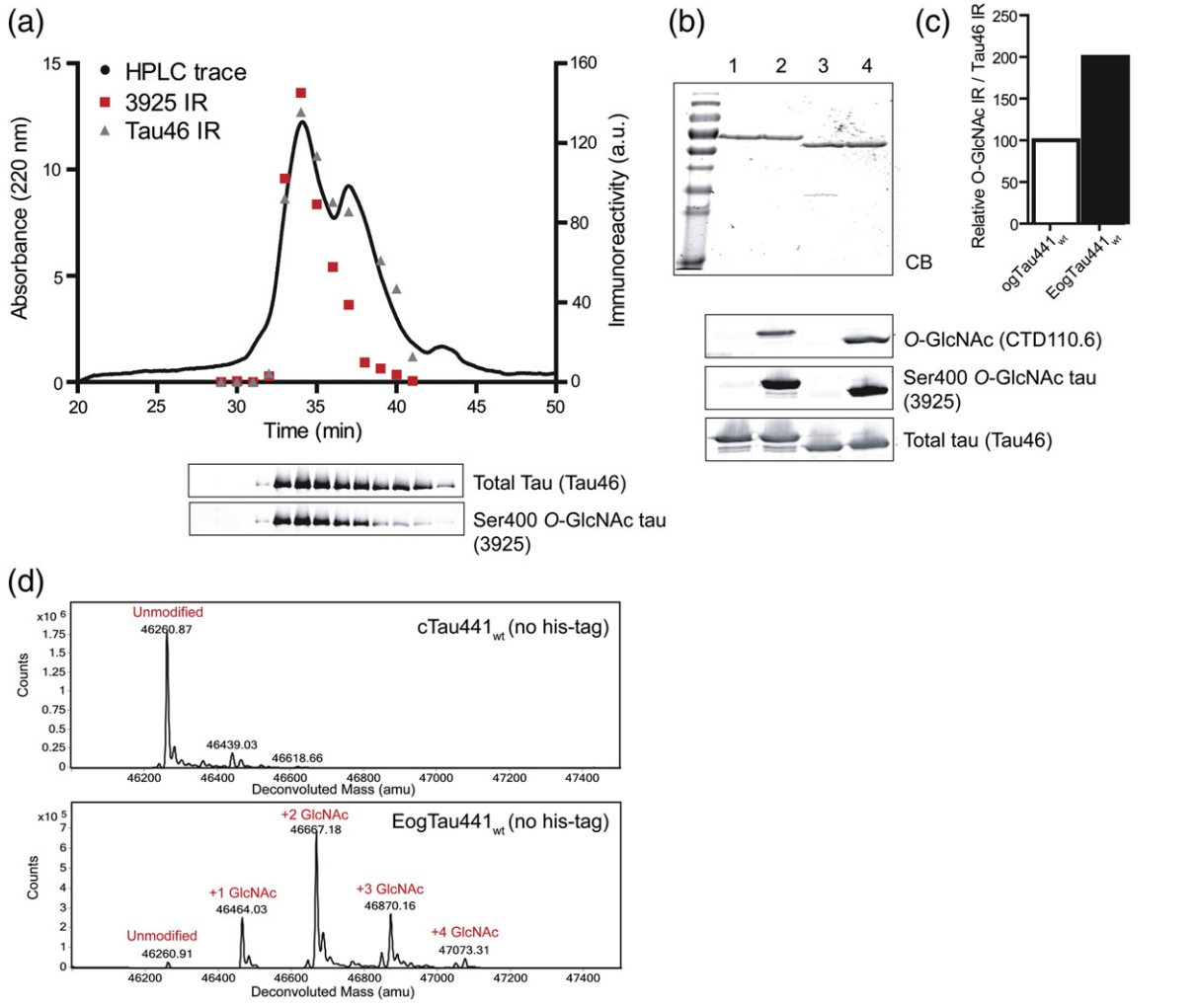

Fig. 3. *O*-GlcNAc-modified Tau441 can be enriched to near stoichiometric quantities. (**a**) ogTau441$_{wt}$ can be separated from unmodified Tau441 by reversed phase HPLC. The black HPLC trace indicates that there are two peaks that elute between 28 and 40 min. Using immunoblot analyses of fractions from this region for total tau and for *O*-GlcNAc [shown in the lower panel and with densitometry plotted in red squares (*O*-GlcNAc) and gray triangles (total tau)], it can be seen that the earlier eluting peak stems from the *O*-GlcNAc-modified Tau441. (**b** and **c**) Characterization of the enriched material compared to ogTau441$_{wt}$ and cTau441$_{wt}$ shows an approximately 2-fold enrichment of *O*-GlcNAc-modified tau (referred to as enriched *O*-GlcNAc Tau441, EogTau441$_{wt}$: Lane 1, cTau441$_{wt}$; Lane 2, ogTau441$_{wt}$; Lane 3, cTau441$_{wt}$; Lane 4, EogTau441$_{wt}$). (**d**) ESI-MS analysis shows that the EogTau441$_{wt}$ material is ~98% *O*-GlcNAc-modified tau and contains almost no unmodified Tau441$_{wt}$.

refer to this sample as enriched ogTau441$_{wt}$ (EogTau441$_{wt}$). Analysis of EogTau441$_{wt}$ by ESI-MS reveals that tau is ~98% *O*-GlcNAc modified (Fig. 3d).

Technical challenges associated with this HPLC enrichment strategy limited the amount of EogTau441$_{wt}$ that could be obtained in high purity. Nevertheless, we were able to produce enough material to compare the aggregation propensities of the EogTau441$_{wt}$ (no His$_6$-tag) and cTau441$_{wt}$ (no His$_6$-tag). We first sought to measure the progress of tau aggregation over a period of 8 days using ThS fluorescence (Fig. 4). Aggregation was monitored over a longer period of time because the limited amount of EogTau441$_{wt}$ necessitated using this material at a concentration of 5 μM with 10 μM heparin. As can be seen in Fig. 5, both EogTau441$_{wt}$ and cTau441$_{wt}$ aggregated with a noticeable lag phase. The appearance of a lag phase compared to ogTau441$_{wt}$ (Fig. 2) likely results from the lower EogTau441$_{wt}$ concentration (5 μM), which is close to the critical concentration for tau aggregation (~2 μM). This behavior has been described previously for other tau constructs, where tau concentrations close to the critical concentration leads to greatly decreased aggregation rates and the emergence of a lag phase [43,45]. When fit to a Gompertz model of growth, the

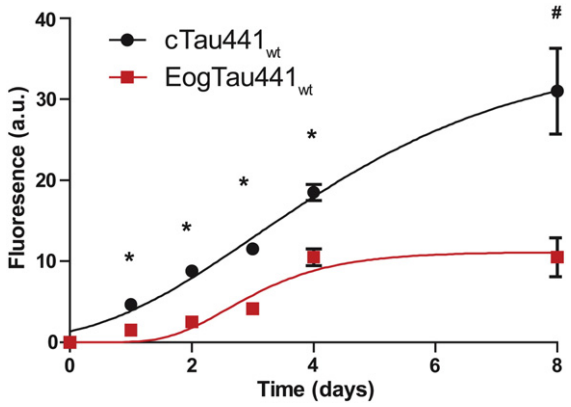

Fig. 4. *O*-GlcNAc modification of Tau441$_{wt}$ slows both nucleation and extension steps of tau aggregation *in vitro*. Aggregation of 5 μM cTau441$_{wt}$ and EogTau441$_{wt}$ (both without His$_6$-tags) in the presence of 10 μM heparin was followed for 8 days using ThS fluorescence. EogTau441$_{wt}$ displays a pronounced lag phase, as well as a significantly lower equilibrium plateau. Error bars represent standard error of the mean and lines represent fits to the Gompertz model. Using a two-tailed student's unpaired *t*-test, (*) indicates $P < 0.005$ and (#) indicates $P < 0.05$.

EogTau441$_{wt}$ exhibited a significantly longer lag time of 1.64 ± 0.64 days compared to 0.47 ± 0.16 days for cTau441$_{wt}$ (Fig. 5). We also noted a 3-fold lower equilibrium position for the EogTau441$_{wt}$ as compared to the cTau441$_{wt}$ sample. Based on the ESI-MS data for EogTau441$_{wt}$ (Fig. 3d), it is evident that this HPLC purification method enriches the doubly and triply *O*-GlcNAc-modified tau species. However, because these aggregation studies are population-based averages, we cannot distinguish the effects of single, double, or triple *O*-GlcNAc modifications of EogTau441$_{wt}$. Indeed, it is possible that sites other than Ser400 may contribute to a greater extent to slowing tau aggregation. Nevertheless, these data indicate that the *O*-GlcNAc on Tau441 slows the nucleation phase of aggregation *in vitro*, as well as impacting the extension or contraction rates of the resulting Tau441 aggregates.

O-GlcNAcylation does not perturb the "global-fold" of Tau441

One possible way in which *O*-GlcNAc on Tau441 might inhibit the nucleation or extension of filaments *in vitro* is by altering its conformation. Such a conformational change could impair formation of fully aggregation competent nuclei. Using Förster resonance energy transfer (FRET) to measure average intermolecular distances between features in the primary structure of tau, Jeganathan *et al*. have shown that tau can adopt a global-fold [46]. In this fold, the C-terminal domain of tau packs close to the microtubule binding repeats and the N-terminal domain packs near the C-terminal domain, thereby creating a "paper-clip" structure [46]. "Pseudophosphorylation" (serine-to-glutamate mutations) mutations of tau at the paired helical filament-1 antibody epitope (pSer396/404) can drive compaction of the paper-clip structure and facilitate tau aggregation *in vitro* [23,46].

Due to the apparent reciprocal relationship between phosphorylation and *O*-GlcNAc on tau observed in the short term upon treatment with inhibitors [27,47], coupled with the effects of Ser396/404 pseudophosphorylation on the global-fold [23], we envisioned a scenario wherein *O*-GlcNAc could hinder compaction of the paper-clip structure and thereby diminish the aggregation propensity of tau. *O*-GlcNAc on tau could, for example, disfavor approach of the C-terminal region of tau toward the microtubule binding repeats and thus inhibit its aggregation. To test this possibility, we generated the Tau441 (C291S/V432W) double mutant, which was previously described by Jeganathan *et al*. [23,46], and then co-expressed this protein in the presence of mutOGT or wtOGT. The control (cTau441$_{C291S/V432W}$) and the *O*-GlcNAc-modified (ogTau441$_{C291S/V432W}$) forms were labeled at the remaining sole cysteine residue (Cys322) with the 1,5-IAEDANS fluorescent probe and then purified by HPLC. The ogTau441*$_{C291S/V432W}$ (* indicating that the protein is labeled with IAEDANS) produced in this manner is both of high purity (Fig. 5a) and *O*-GlcNAc modified (Fig. 5b). During SDS-PAGE analysis, only the samples labeled with IAEDANS showed a fluorescence signal at 336 nm (Fig. 5b, lower panel).

Using these samples, we measured the FRET efficiency between the donor Trp432 and the acceptor IAEDANS-labeled Cys322. A reduction in tryptophan fluorescence at approximately 350 nm and the appearance of an IAEDANS emission band at 490 nm indicated that energy transfer occurred between these two positions as previously reported [46]. We observed similar low FRET efficiencies for both cTau441*$_{C291S/V432W}$ and ogTau441*$_{C291S/V432W}$ from which ensemble-averaged distances of ~36 Å (±17 Å) between the IAEDANS and W432 were calculated (Fig. 5c and d). These distances, determined by assuming the published relationship between FRET efficiency and donor–acceptor separation [46], differ somewhat from the previously reported value of 22.5 Å [46]. The reasons for this difference remain unclear, though they may reflect variations in the sample buffers, concentrations of the analytes, or cuvette path length. Additionally, we cannot eliminate that our purification protocol, which includes HPLC separation, might eliminate the paper-clip structure. We note, however, that formation and stability of the paper-clip structure should be thermodynamically controlled and thus not impacted by the purification protocol. Regardless, when analyzing these data, we observed that *O*-GlcNAc had no effect on the global-fold of tau in solution as measured using these FRET

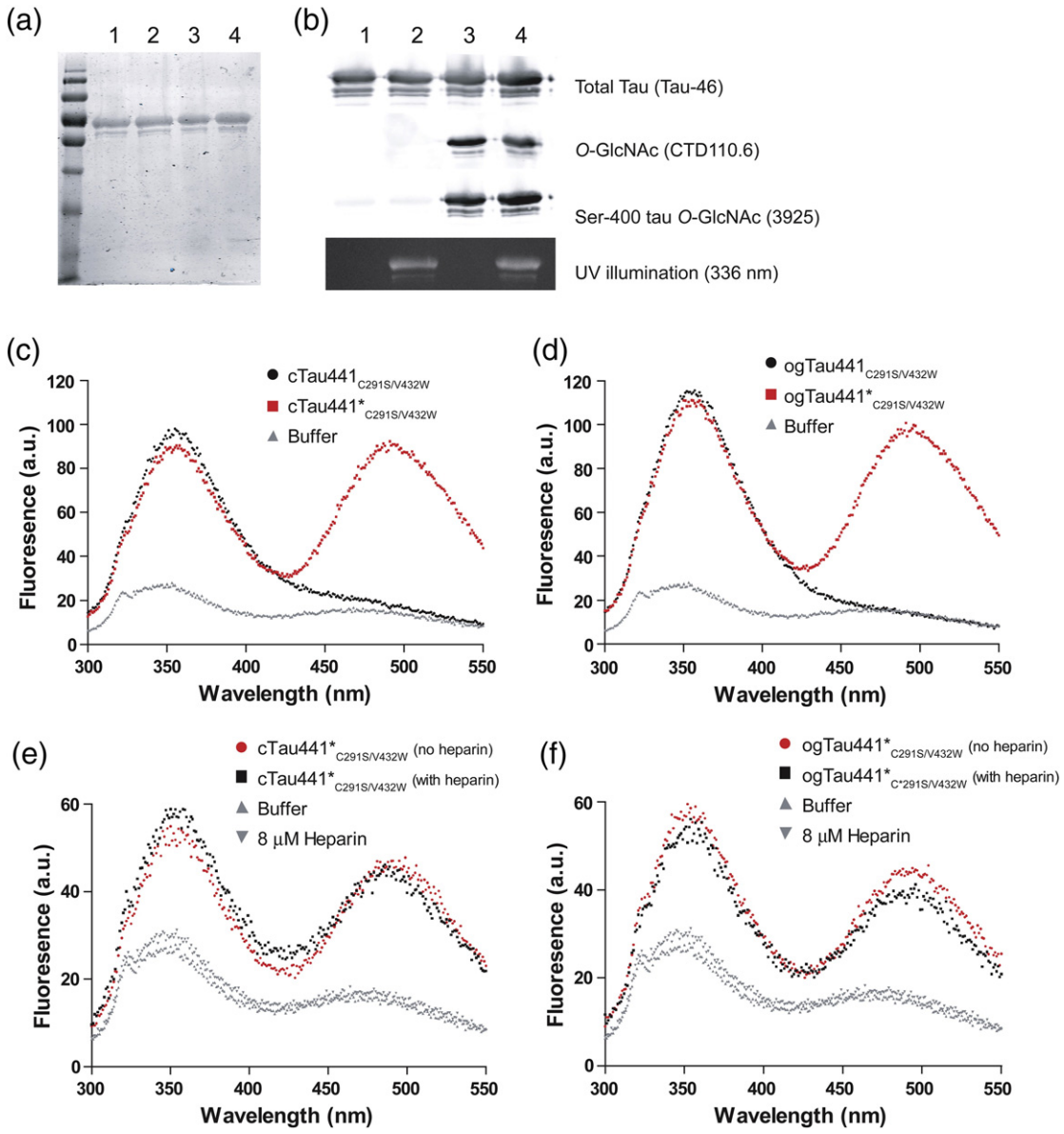

Fig. 5. *O*-GlcNAc modification of Tau441 does not alter the global-fold in solution. (**a**) Coomassie blue-stained SDS-PAGE gel of Lane 1 cTau441$_{C291S/V432W}$ (no IAEDANS), Lane 2 cTau441*$_{C291S/V432W}$ (IAEDANS-modified), Lane 3 ogTau441$_{C291S/V432W}$ (no IAEDANS), Lane 4 ogTau441*$_{C291S/V432W}$ (IAEDANS-modified). (**b**) (top) Total tau immunoblot (Tau-46) indicates equal tau loading in all lanes. (middle) *O*-GlcNAc Western blot with the pan-specific *O*-GlcNAc antibody, CTD110.6, indicates that only ogTau441$_{C291S/V432W}$ and ogTau441*$_{C291S/V432W}$ bear *O*-GlcNAc. The Ser400 *O*-GlcNAc tau antibody, 3925, only detects *O*-GlcNAc on Ser400 on the ogTau441$_{C291S/V432W}$ and ogTau441*$_{C291S/V432W}$ samples. (bottom) Image captured using 336 nm light box indicates that only the IAEDANS-modified samples show fluorescence in an SDS-PAGE gel. (**c** and **d**) Both cTau441*$_{C291S/V432W}$ and ogTau441*$_{C291S/V432W}$ show limited FRET between Trp432 and IAEDANS-labeled Cys322 as evidenced by the minor decrease in tryptophan fluorescence in the presence of the IAEDANS label. (**e** and **f**) The addition of 8 μM heparin to the cTau441*$_{C291S/V432W}$ and ogTau441*$_{C291S/V432W}$ does not result in any increase in FRET between Trp432 and the IAEDANS label at Cys322.

assays. We also added heparin to the FRET samples to assess whether the presence of an inducer of aggregation results in a change in the global-fold. Over the course of 5 min after the addition of heparin, we observed no significant difference between the FRET efficiencies of ogTau441*$_{C291S/V432W}$ and cTau441*$_{C291S/V432W}$ (Fig. 5e and f), indicating that heparin has no measurable effect on the global conformation of tau regardless of its *O*-GlcNAc modification state.

O-GlcNAcylation of Ser400 does not perturb the local conformation or dynamics of Tau353-408

Since we observed no changes in the global-fold of Tau441 due to GlcNAc modification, we used NMR spectroscopy to test the possibility that structural or dynamic perturbations may occur in a more localized manner around the site of modification. However, full-length Tau441 is challenging to study due to its large size and intrinsic disorder, which leads to extensive spectral overlap [48,49]. Accordingly, we turned to a fragment Tau353-408 (residues 353–408) spanning the region from the last microtubule binding repeat to the major GlcNAc-acceptor Ser400 as a model system. This construct is of a sufficiently small size to permit facile spectroscopic analysis while also permitting independent testing of the effects of *O*-GlcNAc on aggregation. cTau353-408 and ogTau353-408 were recombinantly co-expressed with mutOGT or wtOGT, respectively. Both of these peptide fragments were produced as fusions with an N-terminal His_6-SUMO. Expression as a SUMO-fusion protein increased production of recombinant Tau353-408 and facilitated purification of these fusion proteins, as well as facile removal of the affinity tags.

We acquired ^{15}N-heteronuclear single quantum correlation (HSQC) spectra for ^{13}C/^{15}N-labeled

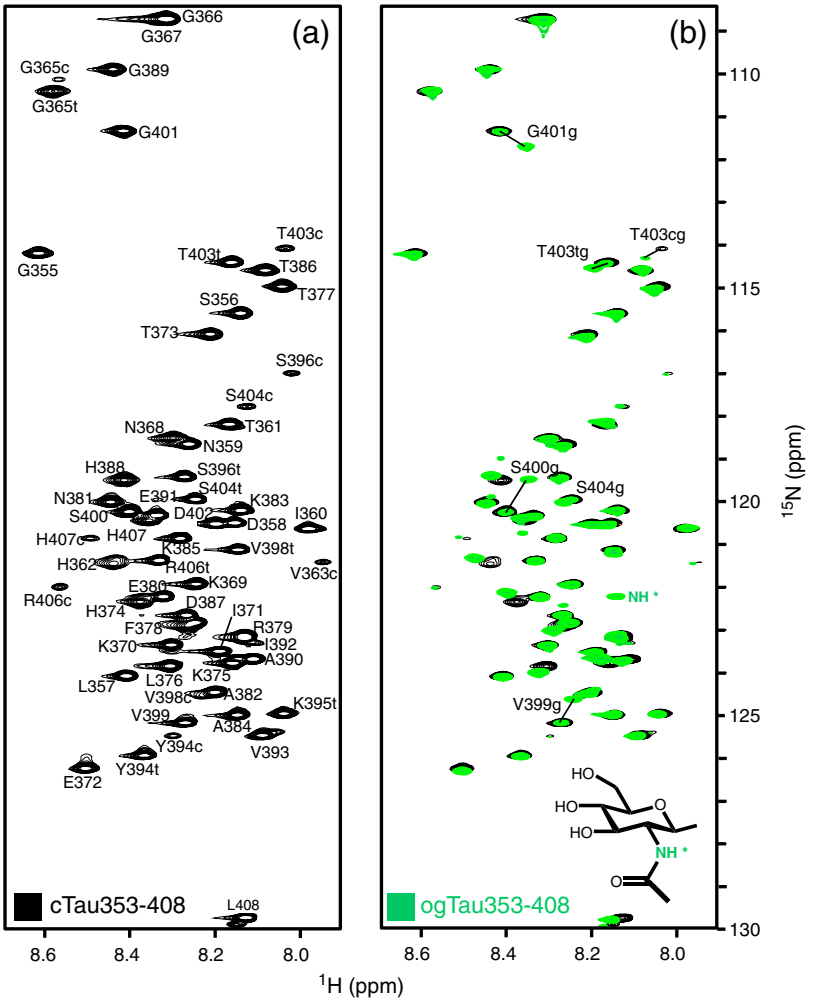

Fig. 6. NMR spectroscopic characterization of Tau353-408. (a) Assigned ^{15}N-HSQC spectrum of cTau353-408. Weak signals from amides in populations of conformers with at least one of three possible *cis* Val363-Pro364, Ser396-Pro397, and Ser404-Pro405 peptide bonds are identified with a "c". The corresponding signals from the major *trans* isomers are identified with a "t". (**b**) Overlaid ^{15}N-HSQC spectra of ogTau353-408 (green) on cTau353-408 (black). The few amides with perturbed chemical shifts are localized near Ser400 and identified with a "g". The GlcNAc amide signal is also detected (NH*). A subset of weaker peaks in the ogTau353-408 spectrum arise from the ~40% unmodified peptide. These assignments are consistent with those reported for a smaller tau fragment (residues 392–411) without and with *O*-GlcNAc modification of Ser400 [35].

cTau353-408 and ogTau353-408 (Fig. 6) and assigned the detected signals for the backbone nuclei using standard heteronuclear correlation approaches. Although HPLC purified, the ogTau353-408 was only ~60% *O*-GlcNAc modified, and thus, a subset of signals corresponding to the unmodified peptide were also present in its ^{15}N-HSQC spectrum. This observation, in effect, provided us with an internal control for studying the modified and unmodified peptides under identical experimental conditions. A comparison of the two spectra showed that only a limited number of amides near Ser400 had perturbed amide $^{1}H^{N}$ and ^{15}N chemical shifts (Fig. 7a). This result both confirmed that Ser400 is the sole site of modification and again indicated that there were no "global" structural changes within this peptide arising from the presence of *O*-GlcNAc. A similar conclusion was reported based on NMR spectroscopic studies of the effects of Ser400 *O*-GlcNAc modification on a smaller tau fragment (residues 392–411) [35].

We calculated the secondary structure propensities of cTau353-408 and ogTau353-408 from main-chain chemical shifts ($^{1}H^{N}$, $^{1}H^{\alpha}$, $^{13}C^{\alpha}$, $^{13}C^{\beta}$, ^{13}CO, and ^{15}N), using the algorithm δ2D, which is specifically calibrated for intrinsically disordered proteins [50]. As summarized in Fig. 7b and Fig. S1, both cTau353-408 and ogTau353-408 are intrinsically disordered with very high overall random coil and some localized polyproline type II helical propensities. Importantly, the presence of *O*-GlcNAc did not change these patterns, except for a very slight increase in predicted β-sheet propensity for residues immediately adjacent

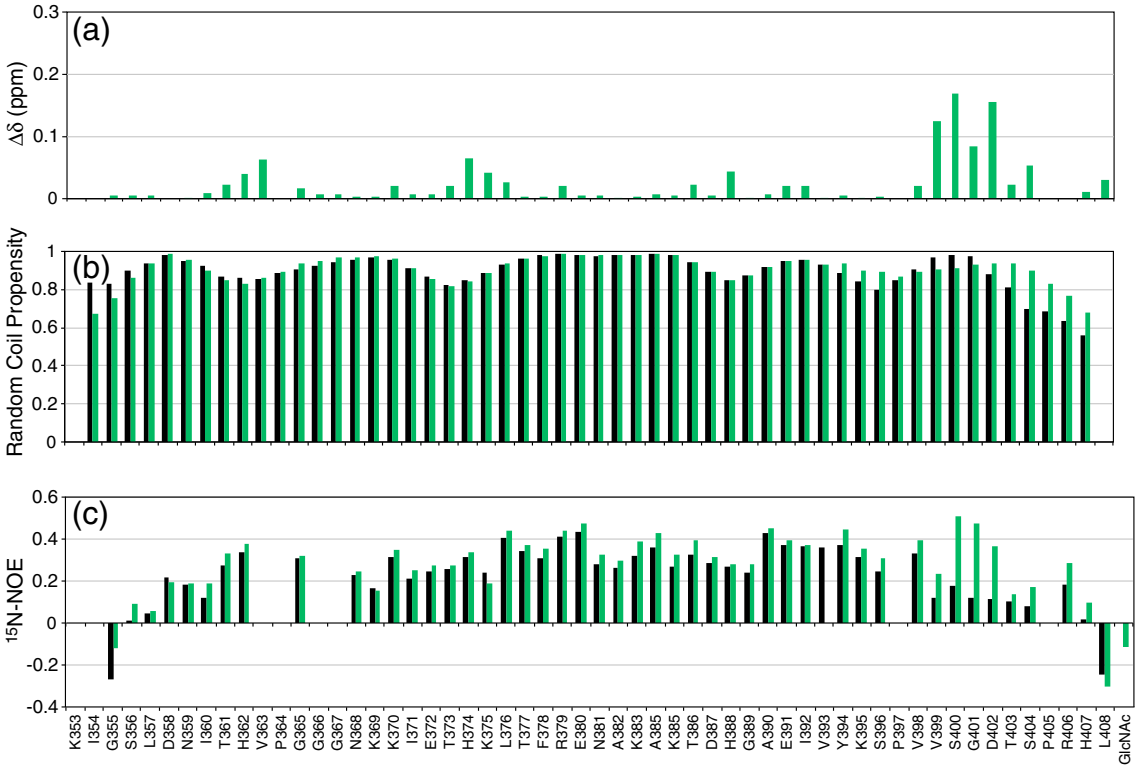

Fig. 7. O-GlcNAcylation **of Ser400 does not perturb the local conformation or dynamics of Tau353-408**. (**a)** Amide chemical shift differences $\{\Delta\delta = [(\Delta\delta_{1H})^2 + (0.2 \times \Delta\delta_{15N})^2]^{1/2}\}$ between the *trans* conformers of ogTau353-408 and cTau353-408. Modest perturbations occurred only near the site of modification. Additional minor chemical shift perturbations clustered around histidine residues. This most likely reflects minor changes in sample pH value, which is close to the pK_a ~ 6 for a histidine side chain. (**b**) Both ogTau353-408 (green) and cTau353-408 (black) have high random-coil propensities based on an analysis of their main-chain chemical shifts with the algorithm δ2D [50]. The small apparent increase in random-coil propensities for the C-terminal residues of ogTau353-408 *versus* cTau353-408 is accompanied by a corresponding decrease in β-strand propensities. See Fig. S1 for the full δ2D analyses. (**c)** Heteronuclear ^{15}N-NOE values of ogTau353-408 (including the GlcNAc amide; green) and cTau353-408 (black). Errors are approximately ±0.05. NOE values decreasing from approximately +0.8 to −3.5 result from increasing mobility of the amide $^{1}H^{N}$–^{15}N bond on the sub-nanosecond timescale, and values ~0.4 are typical for central residues in random-coil peptides when recorded with an 850 MHz NMR spectrometer [51,52]. These measurements show further that both peptides, as well as the GlcNAc, are conformationally dynamic. However, residues near the *O*-GlcNAc-S400 of ogTau353-408 have marginally increased NOE values compared to cTau353-408, suggesting that this modification results slightly in locally increased conformational rigidity on this timescale.

to Ser400 and a decrease for residues toward the C-terminus of the polypeptide (Fig. S1). We believe that this is of questionable significance, given that the algorithm was not calibrated with glycopeptide reference chemical shifts. Also, the backbone φ dihedral angle-dependent $^{3}J_{HN\text{-}H\alpha}$ couplings measured for both cTau353-408 and ogTau353-408 are indicative of random-coil conformations (Fig. S2). In parallel, we also compared the fast sub-nanosecond timescale amide motions of ogTau353-408 and cTau353-408 using heteronuclear ^{15}N-nuclear Overhauser effect (NOE) experiments (Fig. 7c). These measurements supported the conclusion that both peptides are conformationally dynamic. However, residues near the *O*-GlcNAc-modified Ser400 of ogTau353-408 had increased NOE values compared to those in cTau353-408, suggestive of reduced conformational flexibility on the nanosecond-to-picosecond timescale. Collectively, these NMR measurements revealed that Tau353-408 is intrinsically disordered and that the *O*-GlcNAc modification only dampened fast backbone motions in the region immediately surrounding residue 400.

O-GlcNAcylation of Ser400 does not perturb the X-Pro *cis*/*trans* conformational equilibria of Tau

We noted that the ^{15}N-HSQC spectra of cTau353-408 and ogTau353-408 also contained a weak subset of peaks for amides flanking the three proline residues within these fragments (Fig. 6). Based on diagnostic proline $^{13}C^{\beta}$ *versus* $^{13}C^{\gamma}$ chemical shift differences [53], we unambiguously assigned these to a population of conformers with Val363-Pro364, Ser396-Pro397, or Ser404-Pro405 having a *cis* peptide bond (Fig. S3). Notably, Pro397 and Pro405 are proximal to the site of *O*-GlcNAc modification and adjacent to Ser396 and Ser404, both of which are often phosphorylated during tau pathogenesis. Accordingly, we investigated whether the *O*-GlcNAc modification perturbed the *cis*/*trans* ratios for Tau353-408. As summarized in Table S1, the relative populations of the *cis* conformers did not differ significantly between cTau353-408 and ogTau353-408. This observation provided further evidence that the *O*-GlcNAc modification of Ser400 did not measurably alter the conformation of tau.

2.7. Tau-linked *O*-GlcNAc is conformationally dynamic

The ^{15}N-HSQC (Fig. 6) and ^{13}C-HSQC spectra (Fig. S4) of ogTau353-408 also contain well-resolved signals from the *O*-GlcNAc moiety. These signals also allowed us to use NMR methods to investigate mobility of the *O*-GlcNAc residue itself. The heteronuclear ^{15}N-NOE value of the GlcNAc amide is −0.1, demonstrating that this residue is very mobile on the sub-nanosecond timescale (Fig. 7c). Supporting this conclusion, ^{1}H–^{1}H NOEs observed for the GlcNAc acetamido group were only from adjacent protons on the monosaccharide ring and not the protein component of ogTau353-408 (Fig. S4). Therefore, the Ser400-linked *O*-GlcNAc is not conformationally restrained by any non-covalent interactions with the polypeptide.

O-GlcNAcylation also decreases Tau353-408 aggregation propensity

Given that no effects of *O*-GlcNAc on peptide conformation were observed for the Tau353-408 samples beyond the site of modification, we asked whether these truncated proteins showed decreased aggregation propensity as seen for ogTau441. To test this idea, we carried out *in vitro* ThS-monitored aggregation assays using 50 μM cTau353-408 or EogTau353-408 with 12.5 μM heparin. EogTau353-408 was obtained by using a second HPLC purification step and has a higher level (~88%) of *O*-GlcNAc modification. We determined the concentration of the cTau353-408 and EogTau353-408 samples using two different approaches, as outlined in Materials and Methods. With these standardized solutions of the tau fragments, we found that EogTau353-408 both showed a significantly diminished rate of aggregation and reached an ~2.5-fold lower equilibrium value as compared to cTau353-408 when fit to a single exponential growth model (Fig. 8). This result is strikingly similar to that of the corresponding

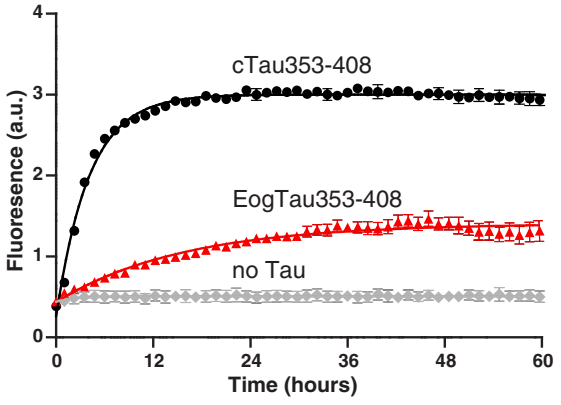

Fig. 8. *O*-GlcNAc modification also inhibits the aggregation of Tau353-408. The aggregation of 50 μM cTau353-408 (black circles) and EogTau353-408 (red triangles) in the presence of 12.5 μM heparin was monitored at 37 °C using ThS fluorescence. The *O*-GlcNAc-modified EogTau353-408 aggregated slower and reached a lower plateau fluorescence value relative than did the unmodified cTau353-408. Also presented is a no protein control (gray diamonds). Average data for triplicates are shown along with error bars representing standard deviations (some error bars are smaller than the symbols). Lines are the bests fit to an exponential growth curve.

EogTau441$_{wt}$ *versus* cTau441$_{wt}$. It is important to note that these measurements were carried out by different personnel in different laboratories, yet both showed that the *O*-GlcNAc modification perturbs the aggregation of full-length tau and a tau fragment containing Ser400.

Conclusions

The *O*-GlcNAc modification has gained increasing attention as its cellular roles are gradually being uncovered. However, the biochemical effects of *O*-GlcNAc modification on most proteins remain unclear. Interest in the function of *O*-GlcNAc on tau has been fueled by recent observations that (i) it occurs within humans with the primary modification site being Ser400 [34–36], (ii) *O*-GlcNAc modification of tau is not found within NFTs [27], (iii) increased *O*-GlcNAc modification in the brain protects against tau-induced neurodegeneration [32], and (iv) *O*-GlcNAc decreases the aggregation propensity of a truncated tau construct [32]. Here we analyzed the biochemical effects of *O*-GlcNAc modification on full-length tau, as well as on a truncated tau construct incorporating Ser400. We find that *O*-GlcNAc on the full-length human isoform of tau does not impact its ability to bind to and stabilize microtubules. However, the modification does inhibit aggregation of full-length Tau441$_{wt}$ *in vitro*. Based on these results, *O*-GlcNAc at Ser400 appears to play a role in hindering tau aggregation. Although not tested in this study, the effect of *O*-GlcNAc at other sites may have similar or even greater effects on aggregation. This inhibition of tau aggregation appeared to be driven principally by slowing the extension phase of aggregation and perturbing the equilibrium position between oligomers and free tau. To evaluate the basis for these effects, we performed biophysical studies on various tau constructs.

Analyses of Tau441 by FRET indicated that there are no gross structural differences between cTau441$_{wt}$ and ogTau441$_{wt}$. Thus, the effect of *O*-GlcNAc does not appear to arise from any ensemble-averaged changes in its global-fold within solution. Analysis of more localized effects of O-GlcNAcylation, performed using a fragment of tau that is readily amenable to NMR spectroscopic analysis, showed that *O*-GlcNAc had no effect on the extent of intrinsic disorder. This conclusion follows from the lack of any substantial changes in the main-chain chemical shifts, $^{3}J_{HN\text{-}H\alpha}$ couplings, and heteronuclear ^{15}N-NOE values of the Tau353-408 fragments, all of which are diagnostic of dynamically averaged random-coil conformations. O-GlcNAcylation of Ser400 also had no obvious effect on the extent of *cis*/*trans* isomerization equilibria of prolines within this tau fragment. We did observe chemical shift perturbations and slightly increased heteronuclear ^{15}N-NOE values for amides adjacent to Ser400, suggesting subtle conformational changes and a dampening of their fast timescale motions within the regions immediately surrounding the site of *O*-GlcNAc modification. However, no interproton NOEs between the *O*-GlcNAc and the polypeptide chain were observed, and ^{15}N-NOE measurements revealed that its amide moiety is also conformationally mobile. Collectively, these experiments demonstrated that O-GlcNAcylation of Ser400 at best only causes small, localized changes to the structure and dynamics cTau353-408. Despite the lack of major effects on tau conformation or dynamics, O-GlcNAcylation of Ser400 dramatically retards the aggregation of both Tau353-408 and full-length tau *in vitro*.

These collective observations are worth considering in light of several existing studies of tau and various glycopeptides. A limited number of NMR-based studies of glycopeptides have indicated that O-glycosylation favors turn conformations in residues flanking the site of modification, possibly through water-mediated hydrogen bonds between the sugar and polypeptide backbone [54–59]. Also, *O*-GalNAc modification of serine and threonine residues of the hinge peptide of serum immunoglobulin A1 reduces the *cis*/*trans* ratio of immediately adjacent proline residues [60]. These effects, however, are likely context dependent and in all cases were localized to the region of modification. The ability of O-GlcNAcylation of Ser400 to influence the aggregation propensity of both Tau441$_{wt}$ and Tau353-408 is therefore remarkable, given that this site is relatively distant from and has no effect on the conformation of the microtubule binding repeats, which are required for tau aggregation.

In the absence of any detectable effects on tau conformation, *O*-GlcNAc modification of tau may decrease its aggregation propensity by enhancing its solubility as seen for keratin [61] or it may also impair its ability to be efficiently incorporated within ordered tau oligomers or otherwise destabilize fibrils into which it is incorporated. The results described here are in clear contrast with the effects of phosphorylation on aggregation of Tau441. For Tau441, pseudophosphorylation increases both the rate of nucleation and the amount of tau fibrils at equilibrium by stabilizing tau fibrils against disassembly [24,25,62]. This work on *O*-GlcNAc therefore highlights the fact that different post-translational modifications of tau can have dramatically different effects on its aggregation *in vitro*. It is also consistent with the observation that these modifications play substantially different roles in the pathogenesis of AD. Modifications such as tau phosphorylation and proteolysis likely provide a driving force for tau-linked neurodegeneration in AD. The *O*-GlcNAc modification, however, may play a protective role in tau biology, and the aggregation of tau in the AD brain might result in part from a failure in such a protective function. Indeed, the results described here, alongside the established protective effects of increased *O*-GlcNAc in transgenic tau

models [32] and the absence of *O*-GlcNAc-modified tau within NFTs [27], support a role for *O*-GlcNAc modification of tau in limiting its aggregation *in vivo*. Collectively, these observations suggest that increased *O*-GlcNAc in the brain may diminish tau toxicity by hindering its ability to form oligomers. This further underscores the potential of this pathway for potential AD therapeutics.

Materials and Methods

O-GlcNAc-modified Tau441 production and purification

pET28a vectors containing the coding sequence of either $Tau441_{wt}$ or $Tau441_{S400A}$ were co-transformed with pMal-c2X vectors encoding wild-type OGT (wtOGT) or H558A OGT (mutOGT) into *E. coli* Tuner cells (Stratagene). To induce expression of $Tau441_{wt}$ or $Tau441_{S400A,}$ we added IPTG (0.5 mM) to the co-transformants, and they were cultured overnight at 22 °C for ~20 h. The bacterial cells were harvested by centrifugation at 5000 rpm for 10 min in a Sorvall RC-6 Plus centrifuge in a FIBERLite F9S-4x1000y rotor. The bacterial pellets were then resuspended in 30 mL of Ni-NTA column binding buffer (20 mM sodium phosphate, 500 mM NaCl, 5 mM imidazole, pH 7.4). Pellets containing wtOGT/$Tau441_{wt}$, mutOGT/$Tau441_{wt}$, wtOGT/$Tau441_{S400A}$, and mutOGT/$Tau441_{S400A}$ were lysed by the addition of 2 mg/mL lysozyme (Bioshop) in the presence of one Roche protease Complete tablet per 30 mL of resuspended bacterial pellet. Disruption of the samples, maintained on ice, was carried out with a Fischer Scientific sonic dismembrator (model 500) using six cycles of 20 s of sonication at 30% power, followed by a 40-s cooling period. Cellular debris were removed by centrifugation at 13,000 rpm in an SS-34 rotor in a Sorvall RC-6 Plus centrifuge. The clarified supernatant from each sample was then loaded onto HisTrap FF Ni-NTA columns (GE Healthcare), which was washed with 90 mL of Ni-NTA column wash buffer (20 mM sodium phosphate, 500 mM NaCl, 60 mM imidazole, pH 7.4) and eluted with 25 mL of Ni-NTA column elution buffer (20 mM sodium phosphate, 500 mM NaCl, 250 mM imidazole, pH 7.4). The eluates were then dialyzed three times against 20 mM sodium phosphate buffer, pH 6.7, and concentrated to 2 mL using an Amicon centrifugal filter.

The Tau441 protein samples (0.25 mg per HPLC run) were acidified using 10% trifluoroacetic acid (TFA) to generate a final TFA concentration of 0.1% (v/v) and loaded onto an Agilent Zorbax 300SB-C8 (9.4 mm × 250 mm) semi-preparative HPLC column housed in an 1100 series Agilent HPLC. The column was held at 30% buffer B [acetonitrile (CH_3CN):water, 0.1% TFA] for the first 5 min, after which the proteins were eluted using a linear gradient of 30–75% CH_3CN over 45 min using a flow rate of 1 mL/min. Fractions (1 mL) were collected using a Foxy Jr. fraction collector over the entirety of the HPLC run, and those containing ogTau441 were pooled and lyophilized to dryness. The $cTau441_{wt}$ and $ogTau441_{wt}$ or $cTau441_{S400A}$ and $ogTau441_{S400A}$ samples were taken up in 1 mL of 20 mM sodium phosphate buffer, pH 7. Samples were assessed for purity by analysis using 12% SDS-PAGE gels, and the concentration of protein in the sample was measured as described below.

Due to some of the unusual physical properties of tau protein, such as its high isoelectric point and the paucity of aromatic amino acids, careful concentration measurements were necessary to avoid systematic errors within these studies. Three different approaches were used to establish equivalent concentrations of the $cTau441_{wt}$, $ogTau441_{wt}$, $cTau441_{S400A}$, and $ogTau_{S400A}$ samples used in the assays. First, the concentration of each of these samples was determined using the Bio-Rad DC assay using BSA (*b*ovine *s*erum *a*lbumin) as a standard, according to the manufacturer's protocol. Based on the results of the DC assay (a *d*etergent-*c*ompatible proprietary modification of the Lowry method), an SDS-PAGE gel was loaded to include equivalent quantities of each of these samples. After staining with Coomassie brilliant blue dye, densitometry of the SDS-PAGE gel confirmed that equivalent quantities of each of these species had indeed been loaded (Fig. 1a). This analysis provided confidence that the concentrations of each of these samples can be measured accurately using the Bio-Rad DC assay. Third, a total tau enzyme-linked immunosorbent assay (ELISA) was developed and used to assay both the $cTau441_{wt}$ and the $ogTau441_{wt}$ samples. The sandwich ELISA involved the use of BT-2 as the tau capture antibody, immobilized on Maxisorp 96-well ELISA plates, followed by use of the Tau-5 tau antibody for detection. Each of these samples was serially diluted from 10,000 pg/mL (based on the DC assay result) down to a concentration of 10 pg/mL, and the signal from the total tau ELISA was determined. This analysis showed that indeed the concentrations of the $cTau441_{wt}$ and the $ogTau441_{wt}$ established using the Bio-Rad DC assay are equivalent within the error of the assays, again giving high confidence that the DC assay provides accurate determinations of the total tau concentration (Fig. S5).

HPLC enrichment of *O*-GlcNAc-modified Tau441

Prior to HPLC enrichment, the $cTau441_{wt}$ and $ogTau441_{wt}$ samples were treated with thrombin (Roche) in a 1:8 (w/w) tau-to-thrombin mass ratio for 20 min at RT (*r*oom *t*emperature). Following cleavage, 1 mM phenylmethylsulfonyl fluoride (PMSF) was added to stop the protease digestions. The $ogTau441_{wt}$ protein (0.25 mg per HPLC run) was acidified using 10% TFA and loaded onto an Agilent Zorbax 300SB-C8 (9.4 mm × 250 mm) semi-preparative HPLC column housed in an 1100 series Agilent HPLC. The proteins were eluted using a linear gradient of 30–35% CH_3CN over 95 min with a flow rate of 1 mL/min. The fractions containing $cTau441_{wt}$ and $ogTau441_{wt}$ were pooled and lyophilized to dryness. The enriched $ogTau441_{wt}$ sample (referred to as $EogTau441_{wt}$) was dissolved in 1 mL of 20 mM sodium phosphate buffer, pH 7, and underwent a second round of HPLC purification. Samples were assessed for their level of purity using 12% SDS-PAGE analysis in conjunction with Coomassie blue staining. The concentration of tau was determined as described above.

Tau353-408 expression and purification

A gene encoding residues 353–408 of tau preceded by His_6-SUMO was cloned into the pET28a plasmid and co-transformed into *E. coli* BL21(λDE3) cells along with

vectors encoding wtOGT and mutOGT, as described above. Unlabeled protein was produced in LB media, whereas M9 minimal media supplemented with 1 g/L $^{15}NH_4Cl$ and/or 3 g/L $^{13}C_6$-glucose was used to produce labeled protein. When the OD_{600} reached 0.6, protein expression was induced with 0.5 mM IPTG, followed by culture growth overnight at 16 ºC. Cells were harvested by centrifugation at 4000*g* in a GSA rotor (Sorvall) for 15 min. After one freeze–thaw cycle, the cell pellet was resuspended in column binding buffer with ~2 mg/mL lysozyme. Cells were then disrupted by sonication (Branson Sonifier 250) at 60% duty cycle until clarified. The cell lysate was spun at 26,000*g* for 60 min in a SS34 rotor (Sorvall). The supernatant was then passed through a 0.8-µm filter before being applied to a 5 mL Ni-NTA column (Qiagen). Once loaded onto the column, it was washed with column binding buffer increased to 30 mM imidazole. The protein was eluted using an ÄKTA Prime Plus FPLC (GE Healthcare) with 100 mL of buffer containing imidazole increased linearly to 250 mM. Fractions containing the desired His_6-SUMO-Tau353-408 were identified by 15% SDS-PAGE gels and pooled.

The His_6-SUMO tag was removed using the catalytic domain of the *Saccharomyces cerevisiae* SUMO hydrolase Ulp1. Cleavage was performed overnight at RT using 5 µg/mL Ulp1 while also dialyzing the protein sample against 20 mM NaH_2PO_4 and 150 mM NaCl, pH 7.0. The resulting cTau353-408, expressed in the presence of mutOGT, was then concentrated and loaded into a 10 × 250 mm semi-preparative C_{18} reversed phase HPLC column (Higgins Analytical, Inc.) and subsequently eluted using a 0–60% CH_3CN gradient (0.1% TFA) at 1 mL/min over 80 min. Fractions (1 mL) were collected with a Gilson FC205 fraction collector, and those containing pure cTau353-408 were pooled and lyophilized. The ogTau353-408 and cTau353-408 mixture, expressed in the presence of wtOGT, was loaded into a 9.4 × 250 mm semi-preparative C_4 column (Agilent) and separated using a 22–27% CH_3CN gradient (0.1% TFA) over 100 min at 1 mL/min. The resulting fractions were analyzed with matrix-assisted laser desorption/ionization time-of-flight mass spectrometry. Samples most enriched in ogTau353-408 were pooled and lyophilized. The same HPLC purification step was repeated to prepare EogTau353-408 (~88% modified and ~12% unmodified). All Tau353-408 samples were resuspended in 10 mM NaH_2PO_4 (pH 6.0), 0.016% protease stock inhibitor tablet (Roche), and 10% D_2O.

The concentrations of the cTau353-408 and ogTau353-408 samples were determined quantitatively through the use of a bicinchoninic acid assay (Thermo Scientific) using BSA as a standard and spectrophotometrically using a NanoDrop 200c absorbance spectrophotometer (Thermo Scientific) with a predicted molar absorptivity ε_{280} of 1490 M^{-1} cm^{-1}. The final concentration for each Tau353-408 sample was taken as the average of these two measurements.

Mass spectrometry of Tau441

Samples were analyzed using an Agilent 6210 LC/MS equipped with an electrospray ionization source (3500 V) and a ZORBAX 300SB-C8 column housed in an Agilent 1100 series HPLC. Proteins (in 20 mM sodium phosphate buffer, pH 7) were loaded onto a pre-equilibrated column using 2% CH_3CN containing 0.1% formic acid for 1 min and then eluted using a linear gradient of 2–60% CH_3CN containing 0.1% formic acid over 12 min. $cTau441_{wt}$ and $ogTau441_{wt}$ eluted at 6.26 and 6.17 min. Extracted total ion chromatograms were deconvoluted using MassHunter workstation software (Agilent) to identify proteins ranging in mass from 46,000 to 49,000 Da. For calculation of the *O*-GlcNAc stoichiometry on $ogTau441_{wt}$, the integration values for the area of each of the *O*-GlcNAc-modified peaks were added and divided by the integration values of all the peaks attributed to tau.

Tubulin polymerization assay

Bovine brain tubulin (>99% purity) was obtained from Cytoskeleton, Inc. (Denver, CO, USA). Tubulin polymerization assays were carried out using 18 µM tubulin, 3 µM Tau441, 2.5 mM GTP, 1 mM dithiothreitol (DTT), 1 mM ethylene glycol bis(β-aminoethyl ether) *N*,*N*′-tetraacetic acid, and 2 mM $MgCl_2$ in 80 mM Pipes, pH 6.9. Tubulin polymerization was monitored by light scattering at 340 nm using a SpectraMax 340 (Molecular Devices).

Immunoblotting

Samples were electrophoresed through 12% SDS-PAGE and transferred to nitrocellulose membranes (Bio-Rad). Membranes were then blocked for 1 h at RT using 2% BSA in PBS (*p*hosphate-*b*uffered *s*aline) containing 0.1% Tween-20 (Sigma) (PBS-T) and subsequently probed overnight at 4 ºC with the appropriate primary antibody in PBS-T plus 2% BSA. Membranes were extensively washed with PBS-T, blocked again for 30 min using 2% BSA in PBS-T at RT, and probed for 1 h at RT with the appropriate HRP (horseradish peroxidase)-conjugated secondary antibody in PBS-T plus 2% BSA. Finally, the membranes were washed extensively with PBS-T and then treated with SuperSignal West Pico Chemiluminescence substrate (Pierce) and exposed to CL-XPosure Film (Pierce) for visualization of immunoreactive protein bands.

Total tau ELISA

We coated 2 µg/mL of the total tau capture antibody BT-2 (Pierce), which recognizes amino acids 194–198 of tau (a region not modified by *O*-GlcNAc), onto wells of Maxisorp ELISA plates (Nunc) in 100 mM sodium bicarbonate/carbonate buffer, pH 9.5, overnight at 4 °C with shaking. On the next day, the capture antibody was aspirated and the plates were blocked with 5% BSA in PBS for 1 h at RT. $cTau441_{wt}$ and $ogTau441_{wt}$ samples, serially 2-fold diluted from 10,000 pg/mL to 10 pg/mL with 1% BSA in PBS, were applied to the plate and incubated for 2 h at RT. After washing five times with PBS-T2 (0.05% Tween), we applied 0.5 µg/mL of a biotinylated total tau Tau-5 detection antibody (Thermo) in 1% BSA in PBS to the plate. This antibody recognizes amino acids 218–225 of tau (a region not modified by *O*-GlcNAc). Five more washes with PBS-T2 were carried out, followed by incubation with 1:10,000 dilution of Streptavidin-HRP (Pierce) in 1% BSA in PBS. Finally, the plate was washed seven times with PBS-T2, and the ELISA was developed using 3,3′,5,5′-tetramethylbenzidine as the substrate for HRP. After quenching by 2 M

H_2SO_4, we read the signal at 450 nm using a SpectraMax 340 plate reader (Molecular Devices).

Tau441 aggregation *in vitro* monitored by ThS

Tau aggregation experiments were performed using 10 μM Tau441 protein (for EogTau441, it was 5 μM tau concentration), 1 mM DTT, 1 mM PMSF, and 0.01 mg/mL thioflavin (ThS) in 20 mM sodium phosphate buffer, pH 7. Reactions were initiated by the addition of 10 μM heparin (5600–6400 Da average molecular weight; International Laboratory, USA) to the reaction mixtures contained in wells of a 96-well fluorescence microplate (Nunc) or a 384-well fluorescence microplate (Corning). The aggregation process was followed by reading the microplate (at the indicated times) in a Molecular Devices Fmax spectrofluorometer using an excitation filter of 440 nm and an emission filter of 520 nm (for 96-well plates) and using a BioTek Synergy4 microplate reading (for 384-well plates). Between readings, the microplate was incubated at 37 ºC in a sealed humidified box to prevent evaporation of water from the aggregation reactions and fresh 1 mM DTT was added every 24 h from a 100 mM stock so as to not significantly dilute the assays. Data were corrected by subtraction of control samples, which contained all of the reaction mixture components except for the tau protein. Experiments were performed in at least triplicate, and data are presented as the ThS fluorescence average ± standard error of the mean. For $Tau441_{wt}$ progress curves, data were fit to either a Gompertz growth function or a one-phase exponential association model using GraphPad Prism 5.03. The Gompertz growth model was used as described previously [42,63]:

$$y = y_m \; e^{-e^{-(t-t_i)^{k\text{app}}}}$$

where y is the fluorescence value measured at time t, y_m is the plateau fluorescence value, t_i is the inflection point when fluorescence is changing most rapidly, and k_{app} is proportional to the rate of polymerization. The lag time is defined as $t_i - 1/k_{app}$.

Tau353-408 aggregation *in vitro* monitored by ThS

Experiments were performed and analyzed as described above, except that samples contained 50 μM Tau353-408 and 12.5 μM heparin in a total of 50 μL. Samples were placed in a black flat-bottom 386-well plate (Grenier), sealed with optically clear crystallography tape (Hampton Research) to limit evaporation, and incubated at 37 °C. The fluorescence of samples was measured every 15 min using a Varioskan Flash fluorimeter (Thermo Scientific).

Tau441 aggregation *in vitro* monitored by filter-trap assay

Tau aggregation studies were performed using 10 μM Tau441 protein, 1 mM DTT, and 1 mM PMSF in 20 mM sodium phosphate buffer, pH 7. Reactions were initiated by the addition of 10 μM heparin to the reaction mixtures. For the time course data, aliquots were removed from each replicate at the indicated time, fixed with 2% glutaraldehyde, quenched with 50 mM Tris, pH 7.6, and then flash frozen and stored at – 80 °C until all of the time points were collected. After 5 days, all of the samples were diluted 20-fold in PBS containing 2% SDS and filtered through a 0.45-μm nitrocellulose membrane (Bio-Rad) that was pre-equilibrated using 2% SDS in PBS. Each well was washed four times using PBS containing 2% SDS, and the membrane was then removed from the apparatus and blocked using PBS containing 1% BSA for 1 h at RT. HT7 primary antibody (0.5 μg/mL) in PBS containing 1% BSA was applied, and the solution was incubated for 1 h at RT. The membrane was then washed with PBS-T three times over 15 min with continual rocking, blocked for 15 min using 1% BSA in PBS, and incubated with 1:1000 IRDye 680LT Goat anti-Mouse IgG (H + L) (Li-Cor) in PBS containing 1% BSA for 1 h at RT in the dark. Following three 15-min washes using PBS-T, we imaged the membrane using the Li-Cor Odyssey and quantified immunoreactivity using Li-Cor Image Studio software.

FRET analysis

The tau FRET experiments were carried out by following as closely as possible the previously published protocol [23,46]. The C291S mutation was introduced into the Tau441 gene contained in the pET28a plasmid using the following primers: 5′-GCAACGTCCAGTCCAAGTCTGGCTCAAAG GATAATATC-3′ and 5′-GATATTATCCTTTGAGCCA GACTTGGACTGGACGTTGC-3′. The V432W mutation was introduced using the following primers: 5′-CCACGC TAGCTGACGAGTGGTCTGCCTCCCTGGCCAAG-3′ and CTTGGCCAGGGAGGCAGACCACTCGTCAGC TAGCGTGG-3′. Both of these mutations were introduced using the Stratagene QuikChange site-directed mutagenesis kit. The plasmids encoding the double mutant were co-transformed with those encoding mutOGT or wtOGT to produce $cTau441_{C291S/V432W}$ or $ogTau441_{C291S/V432W}$, respectively. The resulting co-transformants were cultured in LB media to an OD_{600} of 0.6–0.8, induced using 0.5 mM IPTG for 20 h, and purified by Ni-NTA chromatography, as described above. The resulting $Tau441_{C291S/V432W}$ and $ogTau441_{C291S/V432W}$ samples were reduced using a 5-fold molar excess of TCEP at 37 °C for 15 min. The samples were then incubated for 2 h at RT with a 10-fold molar excess of 1,5-IAEDANS (Invitrogen) dissolved in DMF such that the solution concentration contained a final DMF concentration of 1% (v/v). Following desalting over a PD-10 desalting column (GE Healthcare) to remove excess unreacted 1,5-IAEDANS and the DMF, the $cTau441^*_{C291S/V432W}$ and $ogTau441^*_{C291S/V432W}$ samples were HPLC purified, as described above. Samples were dissolved in 10 mM sodium phosphate buffer, pH 7, and protein concentrations were determined by two independent methods: the Bio-Rad DC assay and confirmed by relative spectrophotometric analysis of the HPLC elution profile monitoring absorbance at 220 nm. Fractional labeling was determined from the HPLC elution profile using the absorbance at 336 nm to quantitate the 1,5-IAEDANS (ε_{336} = 5700 M^{-1} cm^{-1}) relative to the protein concentration. The fractional labeling of tau with 1,5-IAEDANS was 1.0 for the $cTau441^*_{C291S/V432W}$ and was 0.8 for the $ogTau441^*_{C291S/V432W}$. The FRET efficiencies and the resulting intermolecular distances were measured and calculated, respectively, as previously described [23,46].

NMR spectroscopy

NMR data were recorded using an 850 MHz Bruker Avance III spectrometer with samples maintained at 15 ºC in 10 mM sodium phosphate buffer, pH 6.0, with 10% lock D_2O. These conditions were found to be optimal for minimizing signal loss due to amide hydrogen exchange while yielding good quality spectra under near neutral pH conditions. Spectra were processed and analyzed using NMRPipe [64] and Sparky [65], respectively. Main-chain chemical shifts were obtained using CBCA(CO)NH, HNCACB, HNCO, (H)CC(CO)TOCSY-NH, NNH, and HNHA experiments [66,67]. Amide heteronuclear ^{15}N-NOE spectra recorded with or without 5 s of ^{1}H saturation and a total recycle delay of 5 s [68]. The resulting data were fit using the nlinLS routine of NMRPipe [64], and errors were estimated from repeat measurements. Main-chain $^{3}J_{HN\text{-}H\alpha}$ were extracted from HNHA spectra [69]. Interproton NOE measurements were carried out using HNH- and NNH-NOE-HSQC (τ_{mix} = 200 ms) experiments.

Acknowledgements

This research was funded by grants from the Canadian Institutes of Health Research to D.J.V. (MOP 275394) and the Natural Sciences and Engineering Research Council of Canada (NSERC) to L.P.M. Instrument support was provided by the Canadian Institutes of Health Research, the Canada Foundation for Innovation, the British Columbia Knowledge Development Fund, the UBC Blusson Fund, and the Michael Smith Foundation for Health Research. S.A.Y. was supported with scholarships from the Alzheimer Society of Canada and NSERC. D.J.V. thanks the NSERC for support as an E.W.R. Steacie Memorial Fellow and a Canada Research Chair in Chemical Glycobiology.

Appendix A. Supplementary data

Supplementary data to this article can be found online at http://dx.doi.org/10.1016/j.jmb.2014.01.004.

Keywords:
tauopathy;
Alzheimer's disease;
glycosylation;
paired helical filaments;
NMR spectroscopy

† S.A.Y. and A.H.C. contributed equally to this work.

Abbreviations used:
NFT, neurofibrillary tangle; .AD, Alzheimer's disease; OGT, O-GlcNAc transferase; ESI-MS, electrospray ionization mass spectrometry; FRET, Förster resonance energy transfer; HSQC, heteronuclear single quantum correlation; NOE, nuclear Overhauser effect; ThS, Thioflavin-S; TFA, trifluoroacetic acid; NSERC, Natural Sciences and Engineering Research Council of Canada.

References

[1] Oosawa F, Kasai M. A theory of linear and helical aggregations of macromolecules. J Mol Biol 1962;4:10–21.
[2] Congdon EE, Kim S, Bonchak J, Songrug T, Matzavinos A, Kuret J. Nucleation-dependent tau filament formation: the importance of dimerization and an estimation of elementary rate constants. J Biol Chem 2008;283:13806–16.
[3] Friedhoff P, von Bergen M, Mandelkow EM, Davies P, Mandelkow E. A nucleated assembly mechanism of Alzheimer paired helical filaments. Proc Natl Acad Sci U S A 1998;95:15712–7.
[4] Jarrett JT, Berger EP, Lansbury PT. The carboxy terminus of the beta amyloid protein is critical for the seeding of amyloid formation: implications for the pathogenesis of Alzheimer's disease. Biochemistry 1993;32:4693–7.
[5] Wood SJ, Wypych J, Steavenson S, Louis JC, Citron M, Biere AL. alpha-Synuclein fibrillogenesis is nucleation-dependent. Implications for the pathogenesis of Parkinson's disease. J Biol Chem 1999;274:19509–12.
[6] Collins SR, Douglass A, Vale RD, Weissman JS. Mechanism of prion propagation: amyloid growth occurs by monomer addition. PLoS Biol 2004;2:e321.
[7] Chirita CN, Congdon EE, Yin H, Kuret J. Triggers of full-length tau aggregation: a role for partially folded intermediates. Biochemistry 2005;44:5862–72.
[8] Weaver CL, Espinoza M, Kress Y, Davies P. Conformational change as one of the earliest alterations of tau in Alzheimer's disease. Neurobiol Aging 2000;21:719–27.
[9] Alonso A, Zaidi T, Novak M, Grundke-Iqbal I, Iqbal K. Hyperphosphorylation induces self-assembly of tau into tangles of paired helical filaments/straight filaments. Proc Natl Acad Sci U S A 2001;98:6923–8.
[10] Abraha A, Ghoshal N, Gamblin TC, Cryns V, Berry RW, Kuret J, et al. C-terminal inhibition of tau assembly *in vitro* and in Alzheimer's disease. J Cell Sci 2000;113:3737–45.
[11] Wang YP, Biernat J, Pickhardt M, Mandelkow E, Mandelkow EM. Stepwise proteolysis liberates tau fragments that nucleate the Alzheimer-like aggregation of full-length tau in a neuronal cell model. Proc Natl Acad Sci U S A 2007;104:10252–7.
[12] Yin H, Kuret J. C-terminal truncation modulates both nucleation and extension phases of tau fibrillization. FEBS Lett 2006;580:211–5.
[13] Cohen TJ, Guo JL, Hurtado DE, Kwong LK, Mills IP, Trojanowski JQ, et al. The acetylation of tau inhibits its function and promotes pathological tau aggregation. Nat Commun 2011;2:252.
[14] Ledesma MD, Bonay P, Colaco C, Avila J. Analysis of microtubule-associated protein tau glycation in paired helical filaments. J Biol Chem 1994;269:21614–9.
[15] Yan SD, Chen X, Schmidt AM, Brett J, Godman G, Zou YS, et al. Glycated tau protein in Alzheimer disease: a mechanism for induction of oxidant stress. Proc Natl Acad Sci U S A 1994;91:7787–91.

[16] Arnold CS, Johnson GV, Cole RN, Dong DL, Lee M, Hart GW. The microtubule-associated protein tau is extensively modified with *O*-linked *N*-acetylglucosamine. J Biol Chem 1996;271:28741–4.
[17] Kreppel LK, Blomberg MA, Hart GW. Dynamic glycosylation of nuclear and cytosolic proteins. Cloning and characterization of a unique *O*-GlcNAc transferase with multiple tetratricopeptide repeats. J Biol Chem 1997;272:9308–15.
[18] Lubas WA, Frank DW, Krause M, Hanover JA. *O*-Linked GlcNAc transferase is a conserved nucleocytoplasmic protein containing tetratricopeptide repeats. J Biol Chem 1997;272:9316–24.
[19] Dong DL, Hart GW. Purification and characterization of an *O*-GlcNAc selective *N*-acetyl-beta-D-glucosaminidase from rat spleen cytosol. J Biol Chem 1994;269:19321–30.
[20] Gao Y, Wells L, Comer FI, Parker GJ, Hart GW. Dynamic *O*-glycosylation of nuclear and cytosolic proteins: cloning and characterization of a neutral, cytosolic beta-*N*-acetylglucosaminidase from human brain. J Biol Chem 2001;276:9838–45.
[21] Roquemore EP, Chevrier MR, Cotter RJ, Hart GW. Dynamic *O*-GlcNAcylation of the small heat shock protein alpha B-crystallin. Biochemistry 1996;35:3578–86.
[22] Haase C, Stieler JT, Arendt T, Holzer M. Pseudophosphorylation of tau protein alters its ability for self-aggregation. J Neurochem 2004;88:1509–20.
[23] Jeganathan S, Hascher A, Chinnathambi S, Biernat J, Mandelkow EM, Mandelkow E. Proline-directed pseudophosphorylation at AT8 and PHF1 epitopes induces a compaction of the paperclip folding of Tau and generates a pathological (MC-1) conformation. J Biol Chem 2008;283:32066–76.
[24] Necula M, Kuret J. Pseudophosphorylation and glycation of tau protein enhance but do not trigger fibrillization *in vitro*. J Biol Chem 2004;279:49694–703.
[25] Necula M, Kuret J. Site-specific pseudophosphorylation modulates the rate of tau filament dissociation. FEBS Lett 2005;579:1453–7.
[26] Lefebvre T, Ferreira S, Dupont-Wallois L, Bussiere T, Dupire MJ, Delacourte A, et al. Evidence of a balance between phosphorylation and *O*-GlcNAc glycosylation of Tau proteins—a role in nuclear localization. Biochim Biophys Acta 2003;1619:167–76.
[27] Liu F, Iqbal K, Grundke-Iqbal I, Hart GW, Gong CX. *O*-GlcNAcylation regulates phosphorylation of tau: a mechanism involved in Alzheimer's disease. Proc Natl Acad Sci U S A 2004;101:10804–9.
[28] Robertson LA, Moya KL, Breen KC. The potential role of tau protein *O*-glycosylation in Alzheimer's disease. J Alzheimers Dis 2004;6:489–95.
[29] Marshall S, Bacote V, Traxinger RR. Discovery of a metabolic pathway mediating glucose-induced desensitization of the glucose transport system. Role of hexosamine biosynthesis in the induction of insulin resistance. J Biol Chem 1991;266:4706–12.
[30] Taylor RP, Parker GJ, Hazel MW, Soesanto Y, Fuller W, Yazzie MJ, et al. Glucose deprivation stimulates *O*-GlcNAc modification of proteins through up-regulation of *O*-linked N-acetylglucosaminyltransferase. J Biol Chem 2008;283:6050–7.
[31] Heiss WD, Szelies B, Kessler J, Herholz K. Abnormalities of energy metabolism in Alzheimer's disease studied with PET. Ann N Y Acad Sci 1991;640:65–71.
[32] Yuzwa SA, Shan X, Macauley MS, Clark T, Skorobogatko Y, Vosseller K, et al. Increasing *O*-GlcNAc slows neurodegeneration and stabilizes tau against aggregation. Nat Chem Biol 2012;8:393–9.
[33] Lewis J, McGowan E, Rockwood J, Melrose H, Nacharaju P, Van Slegtenhorst M, et al. Neurofibrillary tangles, amyotrophy and progressive motor disturbance in mice expressing mutant (P301L) tau protein. Nat Genet 2000;25:402–5.
[34] Yuzwa SA, Yadav AK, Skorobogatko Y, Clark T, Vosseller K, Vocadlo DJ. Mapping *O*-GlcNAc modification sites on tau and generation of a site-specific *O*-GlcNAc tau antibody. Amino Acids 2011;40:857–68.
[35] Smet-Nocca C, Broncel M, Wieruszeski JM, Tokarski C, Hanoulle X, Leroy A, et al. Identification of *O*-GlcNAc sites within peptides of the Tau protein and their impact on phosphorylation. Mol Biosyst 2011;7:1420–9.
[36] Wang Z, Udeshi ND, O'Malley M, Shabanowitz J, Hunt DF, Hart GW. Enrichment and site mapping of *O*-linked *N*-acetylglucosamine by a combination of chemical/enzymatic tagging, photochemical cleavage, and electron transfer dissociation mass spectrometry. Mol Cell Proteomics 2010;9:153–60.
[37] Geoghegan KF, Dixon HB, Rosner PJ, Hoth LR, Lanzetti AJ, Borzilleri KA, et al. Spontaneous alpha-N-6-phosphogluconoylation of a "His tag" in *Escherichia coli*: the cause of extra mass of 258 or 178 Da in fusion proteins. Anal Biochem 1999;267:169–84.
[38] Aon JC, Caimi RJ, Taylor AH, Lu Q, Oluboyede F, Dally J, et al. Suppressing posttranslational gluconoylation of heterologous proteins by metabolic engineering of *Escherichia coli*. Appl Environ Microbiol 2008;74:950–8.
[39] Du P, Loulakis P, Luo C, Mistry A, Simons SP, LeMotte PK, et al. Phosphorylation of serine residues in histidine-tag sequences attached to recombinant protein kinases: a cause of heterogeneity in mass and complications in function. Protein Expression Purif 2005;44:121–9.
[40] Kim KM, Yi EC, Baker D, Zhang KY. Post-translational modification of the N-terminal His tag interferes with the crystallization of the wild-type and mutant SH3 domains from chicken src tyrosine kinase. Acta Crystallogr Sect D Biol Crystallogr 2001;57:759–62.
[41] Weingarten MD, Lockwood AH, Hwo SY, Kirschner MW. A protein factor essential for microtubule assembly. Proc Natl Acad Sci U S A 1975;72:1858–62.
[42] Winsor CP. The Gompertz curve as a growth curve. Proc Natl Acad Sci U S A 1932;18:1–8.
[43] Friedhoff P, Schneider A, Mandelkow EM, Mandelkow E. Rapid assembly of Alzheimer-like paired helical filaments from microtubule-associated protein tau monitored by fluorescence in solution. Biochemistry 1998;37:10223–30.
[44] Chang E, Kuret J. Detection and quantification of tau aggregation using a membrane filter assay. Anal Biochem 2008;373:330–6.
[45] Ramachandran G, Udgaonkar JB. Evidence for the existence of a secondary pathway for fibril growth during the aggregation of Tau. J Mol Biol 2012;421:296–314.
[46] Jeganathan S, von Bergen M, Brutlach H, Steinhoff HJ, Mandelkow E. Global hairpin folding of tau in solution. Biochemistry 2006;45:2283–93.
[47] Yuzwa SA, Macauley MS, Heinonen JE, Shan X, Dennis RJ, He Y, et al. A potent mechanism-inspired *O*-GlcNAcase inhibitor that blocks phosphorylation of tau *in vivo*. Nat Chem Biol 2008;4:483–90.
[48] Mukrasch MD, Bibow S, Korukottu J, Jeganathan S, Biernat J, Griesinger C, et al. Structural polymorphism of 441-residue tau at single residue resolution. PLoS Biol 2009;7:e34.
[49] Bibow S, Mukrasch MD, Chinnathambi S, Biernat J, Griesinger C, Mandelkow E, et al. The dynamic structure of filamentous Tau. Angew Chem Int Ed 2011;50:11520–4.
[50] Camilloni C, De Simone A, Vranken WF, Vendruscolo M. Determination of secondary structure populations in

disordered states of proteins using nuclear magnetic resonance chemical shifts. Biochemistry 2012;51:2224–31.
[51] Campbell AP, Spyracopoulos L, Irvin RT, Sykes BD. Backbone dynamics of a bacterially expressed peptide from the receptor binding domain of *Pseudomonas aeruginosa* pilin strain PAK from heteronuclear ^{1}H–^{15}N NMR spectroscopy. J Biomol NMR 2000;17:239–55.
[52] Renner C, Schleicher M, Moroder L, Holak TA. Practical aspects of the 2D ^{15}N-{^{1}H}-NOE experiment. J Biomol NMR 2002;23:23–33.
[53] Schubert M, Labudde D, Oschkinat H, Schmieder P. A software tool for the prediction of Xaa-Pro peptide bond conformations in proteins based on ^{13}C chemical shift statistics. J Biomol NMR 2002;24:149–54.
[54] Simanek EE, Huang DH, Pasternack L, Machajewski TD, Seitz O, Millar DS, et al. Glycosylation of threonine of the repeating unit of RNA polymerase II with β-linked *N*-acetylglucosame leads to a turnlike structure. J Am Chem Soc 1998;120:11567–75.
[55] Wu WG, Pasternack L, Huang DH, Koeller KM, Lin CC, Seitz O, et al. Structural study on *O*-glycopeptides: glycosylation-induced conformational changes of *O*-GlcNAc, *O*-LacNAc, *O*-sialyl-LacNAc, and *O*-sialyl-lewis-X peptides of the mucin domain of MAdCAM-1. J Am Chem Soc 1999;121:2409–17.
[56] Chen YX, Du JT, Zhou LX, Liu XH, Zhao YF, Nakanishi H, et al. Alternative *O*-GlcNAcylation/*O*-phosphorylation of Ser(16) induce different conformational disturbances to the N terminus of murine estrogen receptor beta. Chem Biol 2006;13:937–44.
[57] Liang FC, Chen RPY, Lin CC, Huang KT, Chan SI. Tuning the conformation properties of a peptide by glycosylation and phosphorylation. Biochem Biophys Res Commun 2006;342:482–8.
[58] Fernandez-Tejada A, Corzana F, Busto JH, Jimenez-Oses G, Jimenez-Barbero J, Avenoza A, et al. Insights into the geometrical features underlying β-*O*-GlcNAc glycosylation: water pockets drastically modulate the interactions between the carbohydrate and the peptide backbone. Chem Eur J 2009;15:7297–301.
[59] Mallajosyula SS, MacKerell AD. Influence of solvent and intramolecular hydrogen bonding on the conformational properties of O-linked glycopeptides. J Phys Chem B 2011;115:11215–29.
[60] Narimatsu Y, Kubota T, Furukawa S, Morii H, Narimatsu H, Yamasaki K. Effect of glycosylation on cis/trans isomerization of prolines in IgA1-hinge peptide. J Am Chem Soc 2010;132:5548–9.
[61] Srikanth B, Vaidya MM, Kalraiya RD. *O*-GlcNAcylation determines the solubility, filament organization, and stability of keratins 8 and 18. J Biol Chem 2010;285:34062–71.
[62] Chang E, Kim S, Schafer KN, Kuret J. Pseudophosphorylation of tau protein directly modulates its aggregation kinetics. Biochim Biophys Acta 2011;1814:388–95.
[63] Sun Q, Gamblin TC. Pseudohyperphosphorylation causing AD-like changes in tau has significant effects on its polymerization. Biochemistry 2009;48:6002–11.
[64] Delaglio F, Grzesiek S, Vuister GW, Zhu G, Pfeifer J, Bax A. NMRPipe: a multidimensional spectral processing system based on Unix pipes. J Biomol NMR 1995;6:277–93.
[65] Goddard TD, Kneeler DG. Sparky3rd ed. ; 1999.
[66] Sattler M, Schleucher J, Griesinger C. Heteronuclear multidimensional NMR experiments for the structure determination of proteins in solution employing pulsed field gradients. Prog Nucl Magn Reson Spectrosc 1999;34:93–158.
[67] Panchal SC, Bhavesh NS, Hosur RV. Improved 3D triple resonance experiments, HNN and HN(C)N, for H–N and ^{15}N sequential correlations in (^{13}C, ^{15}N) labeled proteins: Application to unfolded proteins. J Biomol NMR 2001;20:135–47.
[68] Farrow NA, Zhang O, Forman-Kay JD, Kay LE. A heteronuclear correlation experiment for simultaneous determination of ^{15}N longitudinal decay and chemical exchange rates of systems in slow equilibrium. J Biomol NMR 1994;4:727–34.
[69] Kuboniwa H, Grzesiek S, Delaglio F, Bax A. Measurement of H-N-H-alpha J-couplings in calcium-free calmodulin using new 2D and 3D water-flip-back methods. J Biomol NMR 1994;4:871–8.